Catalysis Science & Technology

PAPER

View Article Online
View Journal

Cite this: DOI: 10.1039/c7cy00704c

First-principles study of single transition metal atoms on ZnO for the water gas shift reaction

Xiang-Kui Gu,†[a] Chuan-Qi Huang†[a] and Wei-Xue Li *[ab]

Received 11th April 2017,
Accepted 30th May 2017

DOI: 10.1039/c7cy00704c

rsc.li/catalysis

Supported single-atom catalysts have attracted increasing interest due to their high atomic efficiencies and simple structures used to establish the structure–activity relations in catalysis. In this contribution, we present a density functional theory study of ZnO supported single transition metal (TM: Mn, Fe, Co, and Ni) atoms for the water gas shift reaction (WGSR). We find that these single TM_1 atoms prefer to substitute in the surface Zn lattice and exhibit promising activity for stabilizing the intermediates (*i.e.* CO, OH, and COOH) involved in WGSR. Meanwhile, the surface lattice O coordinated with the TM_1 atoms is responsible for the hydrogen abstraction process. The formation of COOH *via* the association between CO and OH is the rate-limiting step in the catalytic cycle. Microkinetic modeling analysis is used to determine the activity trend, and a volcano-like plot between the calculated rates and the binding energies of COOH is obtained, suggesting that the COOH binding energy might be a good activity descriptor for catalyst screening. Among these single atoms, the single Ni_1 atom exhibits the highest activity and is promising for WGSR.

1. Introduction

Single atom catalysts in the form of metals atomically yet uniformly dispersed on metal oxides have attracted considerable interest recently for heterogeneous and electrochemical catalysis.[1–9] These kinds of catalysts can maximize the atomic efficiency and have significant economic benefits. These single atoms are generally stabilized by the lattice oxygen of the oxide supports or alkali metals.[6,10–12] Compared to the nature of the metal atoms in commonly used metal nanoparticles, the properties (particularly oxidation states) of these single metal atoms and the chemical environments around them are very different, consequently affecting the activity/selectivity of the catalytic reactions by means of changing the energetics associated with the elementary steps and/or the reaction pathways. Moreover, the structure of single atom catalysts is simple and well-defined, providing a good platform to develop the structure–reactivity relations in catalysis. Currently, single atom catalysts have been extensively reported, and their promising catalytic performance and stability are observed for various catalytic reactions, such as CO oxidation,[2,13–21] the water gas shift reaction (WGSR),[11,12,22–26] NO reduction,[27,28] steam reforming of hydrocarbons,[10,29] and hydrogenation reactions.[9,30]

Among these reactions, the low temperature WGSR at 200–250 °C is an important process to remove the by-product CO in H_2 from the steam reforming of hydrocarbons[31,32] and provide extra H_2 for fuel cell applications.[33–44] In addition, WGSR is also relevant to several catalytic processes, such as methanol steam reforming,[32,45] syngas conversion,[46] and biomass conversion.[47,48] Generally, two possible reaction mechanisms are proposed for WGSR.[37–39] One is the redox mechanism, in which CO is oxidized by the atomic oxygen from dissociation of water. The other one is the so-called associative mechanism, where CO reacts with OH from water dissociation to form a carboxyl or a formate intermediate followed by dehydrogenation to CO_2. Cu-based catalysts are traditionally used for this reaction, however, Cu suffers from pyrophoricity, sintering, and deactivation during the reaction.[49,50] Alternatively, as mentioned above, single atom catalysts have shown promising performance for this process.[11,12,22–26] Lin *et al.* found that FeO_x supported single Ir_1 atoms exhibit higher activity by almost one order of magnitude as compared to their cluster or nanoparticle counterparts.[22] In addition, the high low-temperature activity of single Pt and Au atoms stabilized by alkali for WGSR was reported by Flytzani-Stephanopoulos and co-workers.[11,12,23,24] They suggested that the active sites are the ensemble composed of single Pt/Au atoms coordinated with oxygen and OH species, and the activities of these single atoms are less dependent on the supports.

Although single atom catalysts have shown potential for low temperature WGSR, the underlying factors that govern

[a] State Key Laboratory of Catalysis, Dalian Institute of Chemical Physics, University of Chinese Academy of Sciences, Chinese Academy of Sciences, Dalian 116023, China
[b] Department of Chemical Physics, College of Chemistry and Materials Science, CAS Center for Excellence in Nanoscience, iChEM, Hefei National Laboratory for Physical Sciences at the Microscale, University of Science and Technology of China, Hefei 230026, China. E-mail: wxli70@ustc.edu.cn
† These authors contributed equally to this work.

their activity towards this reaction are still unclear, making the further optimization of these catalysts challenging. In this work, to shed light on these factors, WGSR is systematically studied on a series of ZnO supported single 3d transition metal (TM = Mn, Fe, Co, and Ni) atoms using density functional theory (DFT) calculations. ZnO is considered as the support because our previous results showed that ZnO nanowire supported single noble metal atoms are active for WGSR to improve the CO_2 selectivity of methanol steam reforming,[10] and it has been widely used as an efficient support for the low temperature WGSR. These 3d transition metals are selected since they could be highly dispersed in ZnO.[51–55] We find that the single TM_1 atoms tend to substitute in the surface Zn lattice, modifying the surface chemistry of ZnO the most. These TM_1 atoms associated with the surface lattice O coordinated with them compose the active site, where the TM_1 atom facilitates the stabilization of CO, OH, and COOH intermediates, while the surface lattice O is responsible for the abstraction of H from H_2O and COOH. In the catalytic cycle of WGSR, it is found that the CO reaction with OH to form COOH is the rate-limiting step. Microkinetic modeling analysis indicates that Ni_1/ZnO exhibits the highest activity towards this process, having the lowest barrier for COOH formation. A volcano-like plot for the calculated rates as a function of the binding energy of COOH is observed, suggesting that the COOH binding energy might be a good activity descriptor to screen optimal single atom catalysts for WGSR.

2. Computational methods

Spin-polarized DFT calculations were performed using the Vienna *ab initio* Simulation Package (VASP)[56,57] based on the projected augmented wave (PAW) method. The exchange–correlation interaction is described by the generalized gradient approximation (GGA) and Perdew–Wang 91 (PW91) functional.[58] The Kohn–Sham equations are solved using a plane wave basis set with a kinetic energy cutoff of 400 eV. The ZnO($11\bar{2}0$) surface, as one of the mainly exposed surfaces for ZnO crystals, is employed as the support. This surface is modeled using a six-layer slab model with a (2 × 1) unit cell, including four Zn atoms and four O atoms in each layer. To model the atomically dispersed TMs, one of the four surface Zn atoms is substituted by the TM atom (Fig. 1). The optimized lattice constants of bulk ZnO are a = 3.28 Å and c = 5.30 Å, consistent with the experimental values of a = 3.25 Å and c = 5.21 Å. A (2 × 2 × 1) k-point mesh is used to sample the surface Brillouin zone, and a 12 Å vacuum is introduced between the repeated slabs along the z-direction. During optimization, the bottom four layers of the ZnO slab are fixed at their bulk position, while the remaining atoms are relaxed until the residual force is less than 0.02 eV $Å^{-1}$. The thicker eight-layer slab and denser (4 × 4 × 1) k-point mesh are examined, and it is found that the variation of the calculated adsorption energy is negligible. The adsorption energies are calculated as $E_{ads} = E_{ad/sub} - E_{ad} - E_{sub}$, where $E_{ad/sub}$, E_{ad}, and E_{sub} are the total energies of the optimized adsorbate/substrate system, the adsorbate in the gas phase, and the clean substrate, respectively. The transition states of the elementary steps are located by the climbing-image nudged elastic band (CI-NEB) method.[59,60]

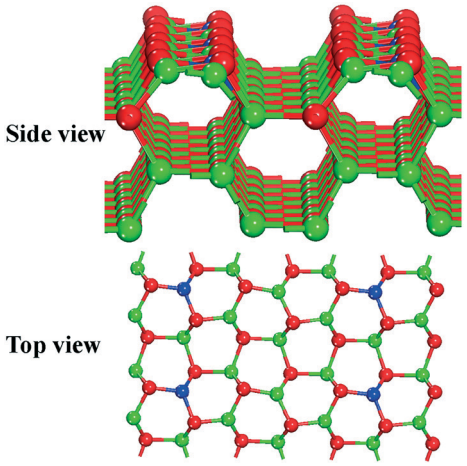

Fig. 1 The side view and top view of the structure of TM_1/ZnO. The green, red, and blue spheres represent the Zn, O, and Mn/Fe/Co/Ni atoms, respectively.

It is well known that DFT methods may not describe well the electronic structures of transition metal oxides, owing to the lack of a reliable exchange–correlation functional for on-site coulomb repulsion between d-electrons. It is preferential to use the DFT+U approach[61] accordingly. Our test calculations showed that when the U value varied from 2.0 to 6.0 eV for Zn, the change of the calculated binding energies of CO and H_2O and the reaction barrier of H_2O dissociation on ZnO is less than 0.10 eV. In addition, compared to the result without U correction, the binding energy difference of CO on Fe_1/ZnO with U = 3.0 eV and J = 1.0 eV for Fe (ref. 62 and 63) is 0.11 eV. These energetics are within the generally accepted accuracy of DFT calculations. Therefore, U correction is not used in the present work, but it still can provide insight into the activity trend.

3. Results and discussion

3.1 Single transition metal atom dispersion on ZnO

Similar to previous findings for ZnO and TiO_2 supported single noble metal atoms,[10,25] the adsorption of single TM atoms on the pristine ZnO surface is unfavorable and they tend to agglomerate. We therefore focus on the substitutional adsorption at the Zn cation lattice in the surface layer or subsurface/bulk region. To study their relative stability, substitution of a TM atom in the first, second, or third ZnO layer is considered. In this particular case, the bottom two layers of the ZnO slab are frozen in their bulk position, and the top four layers are relaxed. The energy differences with respect to the surface-layer substitution are plotted in Fig. 2. For all TMs considered, the energy increases gradually from surface to subsurface/bulk substitution. This suggests that the single

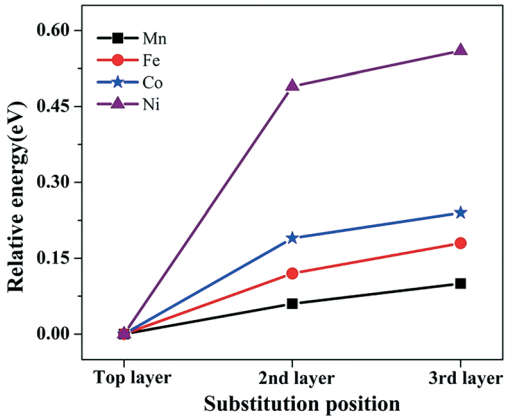

Fig. 2 The relative energies for Mn, Fe, Co, and Ni substituted in the second- and third-layer Zn lattices of ZnO with respect to the surface substitution. The positive value indicates that the corresponding structure is energetically unfavorable.

TM atoms prefer to stay in the surface layer rather than in the subsurface or bulk region, especially for the single Ni_1 atom. These are consistent with previous calculations.[64] The preference for surface substitution may come from the fact that the topmost surface layer has greater freedom to release the structural distortion induced by the substituted TM atoms. Surface substitution being preferable can affect the surface chemistry of ZnO the most. These substituted single TM atoms are positively charged, and the calculated Bader charge decreases gradually from +1.51, +1.40, +1.18 to +1.09 $|e|$ when the TM changes from Mn, Fe, Co, to Ni. Compared with the value of +1.23 $|e|$ for the surface Zn atom, the Bader charges of Mn and Fe are slightly higher, while those of Co and Ni are slightly lower.

The substitution of these single TM atoms can modify the activity of the surface lattice O coordinated with them, as inferred from the formation energy of the surface oxygen vacancy (E_V) with respect to a half O_2 in the gas phase. As compared to the calculated E_V of 2.91 eV for pristine ZnO, the values of 3.21, 3.32, and 3.11 eV for surface O coordinated with Mn, Fe and Co, respectively, are higher. Meanwhile, the value of 2.83 eV for surface oxygen binding to Ni is slightly lower. These results suggest that single Ni_1 atom substitution increases the reducibility of ZnO, however, it decreases for Mn, Fe, and Co substitutions. On the other hand, regardless of these surface substituted 3d TMs, the binding strength of the lattice oxygen with the oxide host remains too strong to be active for CO oxidation at low temperatures. This is in contrast to CeO_2 substituted by the noble metals, where the surface lattice oxygen is activated and active for CO oxidation *via* the Mars–van Krevelen mechanism;[19] consequently WGSR can occur *via* the redox mechanism.[65,66] This implies that the redox mechanism is less favorable for WGSR on these single 3d TM atoms supported on ZnO. Therefore, in the following discussion, we only focus on the associative mechanism.

3.2 Binding energies of reactants and intermediates

The calculated most stable binding energies of the reactants and intermediates involved in WGSR on pristine ZnO and TM_1/ZnO are listed in Table 1, and the corresponding configurations are shown in Fig. 3. On the ZnO surface, CO prefers to adsorb atop of the exposed Zn cation with a weak binding energy of −0.39 eV (Fig. 3a), which agrees with the experimental finding.[67] On TM_1/ZnO, CO prefers to adsorb atop of the single TM_1 atoms (Fig. 3b) and stronger binding strengths are found as compared to that on ZnO. The calculated binding energies are −0.91, −0.77, −1.10, and −0.68 eV on Mn_1, Fe_1, Co_1, and Ni_1, respectively. The enhanced binding for CO adsorption on the TM_1 atoms comes from the high lying 3d-states of the TM atoms, which allow the extensive hybridization with CO orbitals (not shown here). It is clear that the single TM_1 atoms could offer favorable adsorption sites which are otherwise not present on the pristine ZnO surface.

For water adsorption on the ZnO surface, it prefers to occur again at the top of the Zn cation with two H-bonds formed between adsorbed water and the surface lattice oxygen (Fig. 3c). The calculated binding energy is −1.10 eV. On Fe_1, Co_1, and Ni_1/ZnO, the site preference at the top of the Zn cation doesn't change and the binding energies are similar to that on ZnO (Fig. 3d), which are stronger by 0.22–0.37 eV as compared to that for the water binding to the top sites of these TM_1 atoms. On Mn_1/ZnO, we find that the top sites of Mn_1 and Zn are both favorable for water adsorption, exhibiting comparable binding energies. As mentioned above, the metallic Cu is generally considered as the active component for Cu-based catalysts used for low temperature WGSR, while the weak binding energy of water (−0.21 eV (ref. 45)) on Cu might limit water dissociation and the overall activity. The above findings show that TM_1/ZnO catalysts facilitate overcoming this limitation with much stronger binding than Cu.

For atomic H adsorption on pristine ZnO, the calculated binding energy on top of the surface lattice O with a surface lattice OH group formation is −2.37 eV (Fig. 3e), which is significantly stronger by 1.82 eV than the binding energy on the surface Zn top site (−0.55 eV). As discussed above, the substitution of single TM_1 atoms in the surface Zn lattice would change the activity of the lattice O coordinated with them. This is supported by the change of the binding energies of H on these lattice O atoms, where we find that the substitutions

Table 1 The calculated most stable binding energies of the reactants and intermediates involved in WGSR on ZnO and TM_1/ZnO

	Binding energy (eV)				
	Mn_1	Fe_1	Co_1	Ni_1	ZnO
CO	−0.91	−0.77	−1.10	−0.68	−0.39
H_2O	−1.02	−1.04	−1.04	−1.07	−1.10
OH	−3.49	−3.30	−2.87	−2.68	−1.48
H	−2.27	−2.11	−2.40	−2.68	−2.37
COOH	−1.82	−1.69	−2.00	−1.89	—

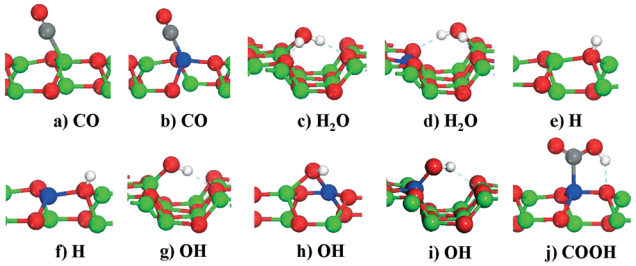

Fig. 3 The most stable configurations of the reactants and various intermediates involved in WGSR on ZnO (a, c, e, and g) and TM_1/ZnO (b, d, f, h, i, and j). It is noted that h) is OH on Mn_1/ and Ni_1/ZnO, while i) is OH on Fe_1/ and Co_1/ZnO. The dashed line denotes the H-bond. The green, red, gray, white, and blue spheres represent the Zn, O, C, H, and Mn/Fe/Co/Ni atoms, respectively.

of Mn_1 and Fe_1 can weaken the binding strength, while an enhancement is observed with Co_1 and Ni_1 substitutions (Table 1). We note that the binding strength of H on these positively charged TM_1 atoms (−1.55–−1.84 eV) remains weaker than that on the lattice O, but much stronger than that on the lattice Zn, suggesting that these TM_1 atoms are more active.

On pristine ZnO, the OH group tends to bind to the top site of Zn, and the calculated binding energy is −1.48 eV (Fig. 3g). On Fe_1/ and Co_1/ZnO, the most favorable sites for OH binding are the top of single Fe_1 and Co_1 atoms (Fig. 3i), with binding energies of −3.30 and −2.87 eV, respectively. Meanwhile on Mn_1/ and Ni_1/ZnO, OH prefers to adsorb at the Mn_1- and Ni_1-Zn bridge (Fig. 3h), and the corresponding binding energies are −3.49 and −2.68 eV. It is clear that the binding strengths on these single TM_1 atoms are much stronger than that on Zn. Moreover, the binding strength decreases gradually as the TM_1 atom changes from Mn, Fe, Co to Ni, following the oxygen affinity trend of these atoms, where Mn exhibits the highest oxygen affinity, while Ni exhibits the lowest.

Trans-carboxyl (COOH), an important intermediate in WGSR, is not stable on the pristine ZnO surface. However, it can be stabilized by the single TM_1 atoms through its carbon atom binding to the top of TM_1 and its –OH group points to the surface lattice oxygen of ZnO to form an H-bond (Fig. 3j). The calculated binding energies are −1.82, −1.69, −2.00, and −1.89 eV on Mn_1, Fe_1, Co_1, and Ni_1 atoms, respectively.

3.3 Water dissociation and reaction with CO

The above results clearly show that TM_1/ZnO exhibits distinguished surface chemistry towards the binding of species as compared to pristine ZnO, which would significantly impact on the energetics associated with the elementary steps, and consequently, the activity of WGSR. For instance, as the first step of WGSR, water dissociation can be dramatically improved by these single TM_1 atoms. On pristine ZnO, we find that a water monomer strongly favors molecular adsorption rather than dissociation, consistent with the literature.[68–70] However, the dissociation of a water monomer occurs on TM_1/ZnO. For water dissociation on Mn_1/ZnO, the initial state is the most stable adsorbed water molecule on the single Mn_1 atom. At the transition state (TS), one of the O–H bonds is elongated by 0.15 Å to take advantage of the hydrogen abstraction (Fig. 4 TS1). On Fe_1/ and Co_1/ZnO, as mentioned above, a water molecule prefers to bind to the Zn top site, but it cannot dissociate at this site. Meanwhile, we find that water dissociation on Fe_1 and Co_1 atoms is facile after water diffusion from Zn to these single atoms. At TS, the length of the breaking O–H bond is ~1.04 Å (Fig. 4 TS2, 3), which is slightly longer by 0.07 Å than that in water. After the O–H bond breaking, the formed OH on the TM_1 atom and the abstracted H can be stabilized by the H-bond formed between them (Fig. 4 TS2, 3). From Mn_1 to Fe_1 and Co_1, the calculated dissociation barrier with respect to the adsorbed water at the most stable site (Mn_1 for Mn_1/ZnO and Zn for Fe_1/ and Co_1/ZnO) increases gradually from 0.42 to 0.55 and 0.66 eV, because the main driving force (binding of OH) decreases accordingly. We note that the relatively lower binding of OH on Ni_1 results in water still having preference for molecular adsorption on Ni_1/ZnO, which is stronger by 0.60 eV than the dissociation.

The efficient coadsorption of reactants CO and water (OH) is a prerequisite to make them react with each other and trigger the WGSR. On pristine ZnO, the adsorption of water is 0.71 eV stronger than that of CO, suggesting that the ZnO surface would be dominated by water, inhibiting CO adsorption and the following WGSR. However, on single Mn_1, Fe_1, and Ni_1 atoms, we find that the adsorption energies of CO and H_2O become comparable. Especially on the Co_1 atom, CO adsorption becomes even stronger by 0.34 eV than the adsorption of water. These indicate that TM_1/ZnO can provide the active sites for the adsorption of both CO and water. More interestingly, we find that on Mn_1/, Fe_1/ and Co_1/ZnO with a pre-adsorbed water monomer, the coming CO would

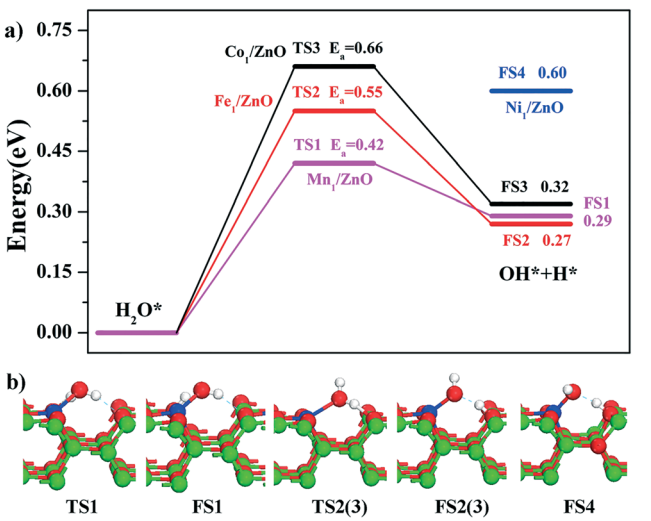

Fig. 4 a) The potential energy profiles for water dissociation on TM_1/ZnO. b) The structures of the optimized transition states (TSs) and final states (FSs).

induce spontaneous dissociation of water, and this process is exothermic by 0.10, 0.28 and 0.45 eV, respectively. For Ni_1/ZnO, CO and H_2O could form a stable coadsorption configuration sharing the single Ni_1 atom with a total adsorption energy of −1.06 eV. The optimized configuration is shown in Fig. 5 IS, where the adsorbed water forms an H-bond with the surface lattice oxygen. The co-adsorbed water could dissociate easily *via* proton transfer along the H-bond by overcoming a small barrier of 0.14 eV, and this reaction is exothermic by 0.28 eV. At the TS (Fig. 5), the bond length of the breaking O–H bond is 1.04 Å and the new H–O bond formed is 1.53 Å. The dissociation of water induced by CO stems from the fact that the O–3d TM_1 bond weakened by coordinating with the coming CO (Fig. 5 IS), which in turn makes the corresponding oxygen more reactive for abstraction of H from the pre-adsorbed water. These results clearly show that CO induced water dissociation is more facile as compared to water direct dissociation. Taking into account the fact that water is more hyperstoichiometric under WGSR conditions in experiments (~22% H_2O *versus* ~7% CO),[41] CO induced water dissociation is dominant for WGSR, and the direct dissociation of water *via* water diffusion from the Zn atoms to the TM_1 atoms has a limited effect on the activity of this reaction.

The independence on the single TM_1 atoms considered, the final configurations of the dissociated water induced by CO are similar (Fig. 5 FS). Co-adsorbed CO and OH from H_2O both coordinate with the single TM_1 atoms, similar to that on ZnO supported single noble atoms.[10] The abstracted H in the surface lattice OH formed can desorb from the surface easily in the form of H_2, which will be discussed later. OH tilts left toward the neighboring Zn to coordinate with the TM_1-Zn bridge, and the resulting configuration with CO (Fig. 6 IS) is the precursor for the formation of the *trans*-carboxyl (COOH). To form the (O)C–O(H) bond, the OH at the bridge site is raised upward to break the Zn–O(H) bond and shares the single TM_1 atom with CO at the TS (Fig. 6 TS).

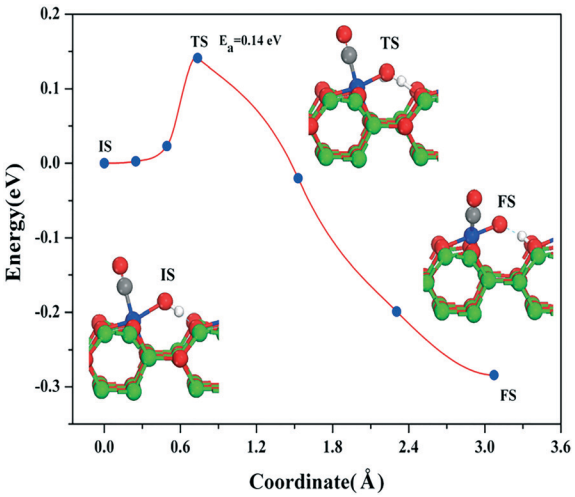

Fig. 5 The potential energy profile of CO induced water dissociation on Ni_1/ZnO. The insets are the optimized structures of the initial state (IS), transition state (TS), and final state (FS), respectively.

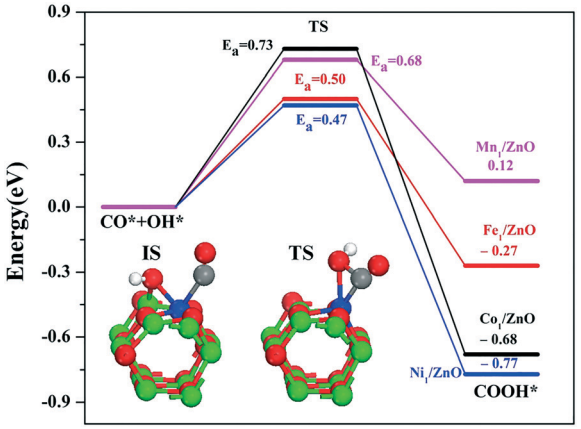

Fig. 6 The potential energy profiles of CO reaction with OH to form *trans*-COOH on TM_1/ZnO. The insets are the optimized structures of the co-adsorbed CO and OH (IS) and the transition state (TS).

The calculated barriers for COOH formation are 0.68, 0.50, 0.73, and 0.47 eV on Mn_1, Fe_1, Co_1, and Ni_1, respectively. This process on Mn_1/ZnO is slightly endothermic (0.12 eV) due to the stronger binding of OH (Table 1), while on Fe_1/, Co_1/, and Ni_1/ZnO, it is exothermic by 0.27, 0.68, and 0.77 eV, respectively.

3.4 CO_2 and H_2 formation

The potential energy profiles for the dehydrogenation of the *trans*-COOH to produce CO_2 on TM_1/ZnO are shown in Fig. 7. The calculated barriers for this step are 0.24, 0.05, 0.07, and 0.02 eV on Mn_1, Fe_1, Co_1, and Ni_1, respectively, which are small and significantly lower than that on the commonly used Cu catalyst for WGSR, for instance, 1.41 eV on Cu(111).[37] The facile dehydrogenation stems from the formation of a H-bond between the *trans*-COOH and surface lattice oxygen (Fig. 3j). At the TS (Fig. 7 TS), the length of the O–H bond in the *trans*-COOH is elongated by 0.31 Å on Mn_1/ZnO, while it is elongated by 0.13, 0.16 and 0.07 Å on Fe_1, Co_1, and

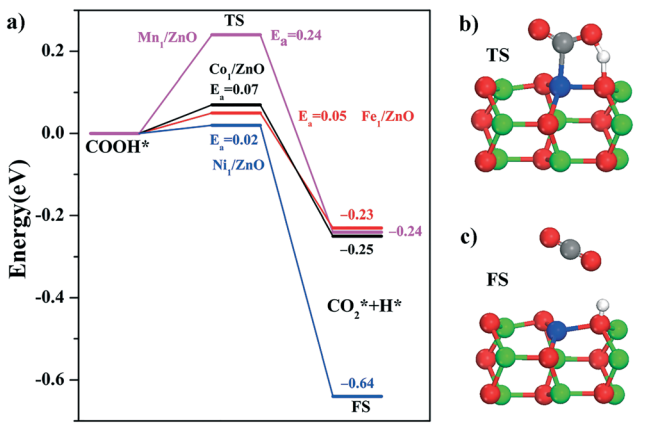

Fig. 7 a) The potential energy profiles of *trans*-COOH dehydrogenation to CO_2 and H on TM_1/ZnO. b) and c) are the structures of the transition state (TS) and final state (FS), respectively.

Ni_1, respectively. After the breaking of the O–H bond (Fig. 7 FS), the produced CO_2 readily desorbs from the surface left with produced surface lattice OH. This step is exothermic by ~0.25 eV on Mn_1, Fe_1, and Co_1/ZnO, and 0.64 eV on Ni_1/ZnO.

H_2 formation is the final step in the catalytic cycle of WGSR. We find that hydrogen association from the surface lattice OH to form H_2 in the gas phase is thermodynamically very facile. This is because the dissociative adsorption of H_2 is very weak on the systems considered, and the calculated dissociative binding energies (with respect to a half H_2 in the gas phase) are −0.10, 0.00, 0.16, −0.13, and −0.41 eV on pristine ZnO, Mn_1/, Fe_1/, Co_1/, and Ni_1/ZnO, respectively. In addition, taking into account the entropy contribution of H_2 in the gas phase, desorption of one H_2 molecule from the surface into the gas phase will release about 0.62 eV at 473 K and standard pressure, which is sufficiently large to overcome the binding of hydrogen on the surfaces.

3.5 Activity trend for WGSR on ZnO supported single atoms

From the above, we know that the catalytic cycle of WGSR on TM_1/ZnO tends to be closed *via* the associative mechanism, involving the elementary steps of water and CO adsorption, water dissociation, CO reaction with OH to form COOH, COOH dehydrogenation to CO_2, and hydrogen desorption, as described in eqn (1)–(6).

$$CO + * \rightleftharpoons CO* \quad (1)$$

$$H_2O + * \rightleftharpoons H_2O* \quad (2)$$

$$H_2O* + * \rightleftharpoons OH* + H* \quad (3)$$

$$CO* + OH* \rightleftharpoons COOH* + * \quad (4)$$

$$COOH* \rightleftharpoons CO_2 + H* \quad (5)$$

$$2H* \rightleftharpoons H_2 + 2* \quad (6)$$

In this cycle, the adsorbed water on Mn_1/, Fe_1/, and Co_1/ZnO could dissociate directly by overcoming a modest barrier or being spontaneously induced by the co-adsorbed CO. On Ni_1/ZnO, the co-adsorbed CO also facilitates the dissociation of water by overcoming a small barrier of 0.14 eV. The dissociation of water induced by CO is exothermic on all single TM_1 atoms considered. The CO and OH co-adsorbed at the single TM_1 atoms readily react with each other and form the *trans*-COOH, and the elementary processes are exothermic (Fe_1, Co_1, and Ni_1) or only slightly endothermic (Mn_1). The *trans*-COOH formed can easily dehydrogenate (exothermic) and release CO_2. The association of hydrogen to produce H_2 in the gas phase is facile due to the weak dissociative binding energy of hydrogen on TM_1/ZnO. The rate-limiting step is the COOH formation, which exhibits the highest barrier in the catalytic cycle with calculated values of 0.68, 0.50, 0.73, and 0.47 eV on Mn_1, Fe_1, Co_1, and Ni_1/ZnO, respectively. The active site of TM_1/ZnO is composed of the single TM_1 atom and the coordinated surface lattice oxygen. The TM_1 atom can stabilize CO, OH, and COOH intermediates, while the surface lattice oxygen is responsible for hydrogen abstraction from H_2O and COOH.

Based on the energetics associated with the eqn (1)–(6), microkinetic modeling analysis is used to calculate the rates toward WGSR on TM_1/ZnO. Quasi-equilibrium and steady-state approximations are used to determine the coverages of intermediates and the vacant sites. The rate constants for all the catalytic reactions are expressed as:

$$k = \frac{k_b T}{h} \exp(-E_a/RT) \quad (7)$$

where k_b, h and E_a are the Boltzmann constant, Planck constant and activation energy barrier, respectively. The simulated reaction conditions are 473 K and standard pressure with a feed composition of 7% CO, 21% H_2O, 8.5% CO_2, and 38% H_2, balanced with inert gas.[37] We assume that the entropy contributions of CO/H_2O adsorption and CO_2/H_2 desorption are mostly from the contribution of the translational entropy, which is calculated using a reported method.[48] We estimate that, under these reaction conditions, CO and H_2O in the gas phase lose 0.78 and 0.76 eV of entropic free energy when adsorbing, while CO_2 and H_2 desorption can gain 0.81 and 0.62 eV, respectively. Fig. 8 shows that the single Ni_1 atom exhibits the highest activity, because it has the lowest barrier for COOH formation (the rate-limiting step). Meanwhile, the higher barriers for this reaction on the single Mn_1 and Co_1 atoms result in lower activity as compared to the Ni_1 atom. We note that, although the barrier for COOH formation on the single Fe_1 atom is just slightly higher than that on Ni_1, the Fe_1 atom exhibits the lowest activity. This is because the coverage of CO on Fe_1 atoms is very low because the binding strength of CO on Fe_1 is the weakest compared to those on the other single atoms. Moreover, a volcano-like relationship[71] between the calculated rates and the binding

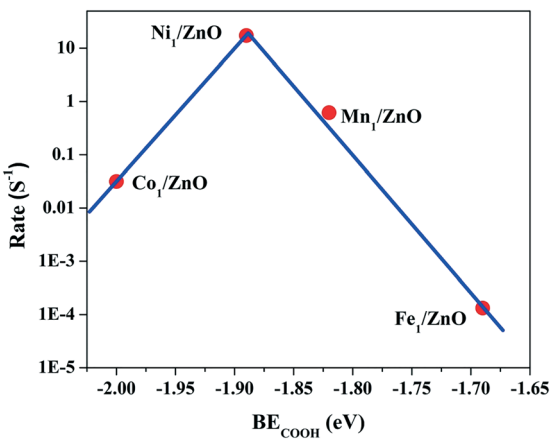

Fig. 8 Volcano-like relationship between calculated rates for the water gas shift reaction on TM_1/ZnO and the binding energies of COOH intermediates.

energies of COOH is found (Fig. 8), suggesting that the binding energy of COOH might be an activity descriptor to screen optimal single atom catalysts of transition metals for WGSR.

From the above, we know that the active site of the oxide supported single TM_1 catalysts is the ensemble of the single TM_1 atoms and the coordinated surface lattice O, which facilitates water adsorption and dissociation. Moreover, the formation of the COOH intermediate is the rate-limiting step in the catalytic cycle of WGSR. Similar catalytic behaviors are also reported for WGSR on the metal/oxide interfaces, where water activation is very facile and COOH formation controls the overall activity the most.[41,44] These two kinds of active sites are more favorable for WGSR, as compared to that on the TM surfaces, where weak water adsorption would limit the activity of water dissociation and WGSR.[37,39] On the other hand, different from the site separation for CO and H_2O/OH adsorption at the metal/oxide interfaces, these intermediates favor sharing the same single TM_1 atoms on the single atom catalysts, implying that, to achieve high overall performance of WGSR, the intrinsic activity of the TM_1 atom should be high enough to bind the species. Furthermore, the concentration of the single TM_1 atom should be high, which is the current challenge for single atom catalysts.

4. Conclusions

Spin-polarized DFT calculations are employed to systemically study the water gas shift reaction on ZnO supported single Mn_1, Fe_1, Co_1, and Ni_1 atom catalysts. It is found that these single atoms substituted in the surface Zn lattice are energetically most favorable, and therefore, can efficiently tune the surface chemistry of ZnO with high catalytic activity. The active site of these single atom catalysts is composed of the single TM_1 atom and the neighboring surface lattice O. The single TM_1 atom plays a role of stabilizing CO, OH, and COOH intermediates, and the surface lattice O is responsible for hydrogen abstraction from H_2O and COOH. We find that the CO reaction with OH to form COOH is the rate-limiting step, with the highest barrier in the catalytic cycle. Based on microkinetic modeling analysis, it is found that the single Ni_1 atom exhibits the highest activity. Moreover, a volcano-like relationship between the calculated rates and the binding energies of COOH is found, suggesting that the binding energy of COOH might be an activity descriptor to screen the optimal single-atom catalysts for the water gas shift reaction.

Acknowledgements

This work received financial support from the National Natural Science Foundation of China (91645202 and 21321002), the National Basic Research Program of China (2013CB834603), and the National Key Research and Development Program of China (2017YFB0602200).

References

1 J. Y. Liu, *ACS Catal.*, 2017, **7**, 34–59.
2 Y. G. Wang, D. H. Mei, V. A. Glezakou, J. Li and R. Rousseau, *Nat. Commun.*, 2015, **6**, 6511.
3 X. F. Yang, A. Q. Wang, B. T. Qiao, J. Li, J. Y. Liu and T. Zhang, *Acc. Chem. Res.*, 2013, **46**, 1740–1748.
4 S. Yang, Y. J. Tak, J. Kim, A. Soon and H. Lee, *ACS Catal.*, 2017, **7**, 1301–1307.
5 C. H. Choi, M. Kim, H. C. Kwon, S. J. Cho, S. Yun, H. T. Kim, K. J. J. Mayrhofer, H. Kim and M. Choi, *Nat. Commun.*, 2016, **7**, 10922.
6 C. Y. Wang, M. Yang and M. Flytzani-Stephanopoulos, *AIChE J.*, 2016, **62**, 429–439.
7 R. Lang, T. B. Li, D. Matsumura, S. Miao, Y. J. Ren, Y. T. Cui, Y. Tan, B. T. Qiao, L. Li, A. Q. Wang, X. D. Wang and T. Zhang, *Angew. Chem., Int. Ed.*, 2016, **55**, 16054–16058.
8 J. Jones, H. F. Xiong, A. T. Delariva, E. J. Peterson, H. Pham, S. R. Challa, G. S. Qi, S. Oh, M. H. Wiebenga, X. I. P. Hernandez, Y. Wang and A. K. Datye, *Science*, 2016, **353**, 150–154.
9 G. Kyriakou, M. B. Boucher, A. D. Jewell, E. A. Lewis, T. J. Lawton, A. E. Baber, H. L. Tierney, M. Flytzani-Stephanopoulos and E. C. H. Sykes, *Science*, 2012, **335**, 1209–1212.
10 X. K. Gu, B. T. Qiao, C. Q. Huang, W. C. Ding, K. J. Sun, E. S. Zhan, T. Zhang, J. Y. Liu and W. X. Li, *ACS Catal.*, 2014, **4**, 3886–3890.
11 M. Yang, J. L. Liu, S. Lee, B. Zugic, J. Huang, L. F. Allard and M. Flytzani-Stephanopoulos, *J. Am. Chem. Soc.*, 2015, **137**, 3470–3473.
12 M. Yang, S. Li, Y. Wang, J. A. Herron, Y. Xu, L. F. Allard, S. Lee, J. Huang, M. Mavrikakis and M. Flytzani-Stephanopoulos, *Science*, 2014, **346**, 1498–1501.
13 B. T. Qiao, A. Q. Wang, X. F. Yang, L. F. Allard, Z. Jiang, Y. T. Cui, J. Y. Liu, J. Li and T. Zhang, *Nat. Chem.*, 2011, **3**, 634–641.
14 Z. Y. Li, Z. Yuan, X. N. Li, Y. X. Zhao and S. G. He, *J. Am. Chem. Soc.*, 2014, **136**, 14307–14313.
15 J. X. Liang, J. Lin, X. F. Yang, A. Q. Wang, B. T. Qiao, J. Y. Liu, T. Zhang and J. Li, *J. Phys. Chem. C*, 2014, **118**, 21945–21951.
16 E. J. Peterson, A. T. Delariva, S. Lin, R. S. Johnson, H. Guo, J. T. Miller, J. H. Kwak, C. H. F. Peden, B. Kiefer, L. F. Allard, F. H. Ribeiro and A. K. Datye, *Nat. Commun.*, 2014, **5**, 4885.
17 F. Y. Li, Y. F. Li, X. C. Zeng and Z. F. Chen, *ACS Catal.*, 2015, **5**, 544–552.
18 M. Moses-DeBusk, M. Yoon, L. F. Allard, D. R. Mullins, Z. L. Wu, X. F. Yang, G. Veith, G. M. Stocks and C. K. Narula, *J. Am. Chem. Soc.*, 2013, **135**, 12634–12645.
19 C. L. Wang, X. K. Gu, H. Yan, Y. Lin, J. J. Li, D. D. Liu, W. X. Li and J. L. Lu, *ACS Catal.*, 2017, **7**, 887–891.
20 B. T. Qiao, J. X. Liu, Y. G. Wang, Q. Q. Lin, X. Y. Liu, A. Q. Wang, J. Li, T. Zhang and J. Y. Liu, *ACS Catal.*, 2015, **5**, 6249–6254.
21 B. Long, Y. Tang and J. Li, *Nano Res.*, 2016, **9**, 3868–3880.
22 J. Lin, A. Q. Wang, B. T. Qiao, X. Y. Liu, X. F. Yang, X. D. Wang, J. X. Liang, J. X. Li, J. Y. Liu and T. Zhang, *J. Am. Chem. Soc.*, 2013, **135**, 15314–15317.

23 Y. P. Zhai, D. Pierre, R. Si, W. L. Deng, P. Ferrin, A. U. Nilekar, G. W. Peng, J. A. Herron, D. C. Bell, H. Saltsburg, M. Mavrikakis and M. Flytzani-Stephanopoulos, *Science*, 2010, **329**, 1633–1636.
24 M. Yang, L. F. Allard and M. Flytzani-Stephanopoulos, *J. Am. Chem. Soc.*, 2013, **135**, 3768–3771.
25 S. C. Ammal and A. Heyden, *ACS Catal.*, 2017, **7**, 301–309.
26 W. Y. Song and E. J. M. Hensen, *ACS Catal.*, 2014, **4**, 1885–1892.
27 W. C. Ding, X. K. Gu, H. Y. Su and W. X. Li, *J. Phys. Chem. C*, 2014, **118**, 12216–12223.
28 L. Wang, S. R. Zhang, Y. Zhu, A. Patlolla, J. J. Shan, H. Yoshida, S. Takeda, A. I. Frenkel and F. Tao, *ACS Catal.*, 2013, **3**, 1011–1019.
29 R. B. Duarte, F. Krumeich and J. A. van Bokhoven, *ACS Catal.*, 2014, **4**, 1279–1286.
30 H. S. Wei, X. Y. Liu, A. Q. Wang, L. L. Zhang, B. T. Qiao, X. F. Yang, Y. Q. Huang, S. Miao, J. Y. Liu and T. Zhang, *Nat. Commun.*, 2014, **5**, 5634.
31 R. M. Navarro, M. A. Pena and J. L. G. Fierro, *Chem. Rev.*, 2007, **107**, 3952–3991.
32 D. R. Palo, R. A. Dagle and J. D. Holladay, *Chem. Rev.*, 2007, **107**, 3992–4021.
33 J. A. Rodriguez, J. Graciani, J. Evans, J. B. Park, F. Yang, D. Stacchiola, S. D. Senanayake, S. G. Ma, M. Perez, P. Liu, J. F. Sanz and J. Hrbek, *Angew. Chem., Int. Ed.*, 2009, **48**, 8047–8050.
34 J. B. Park, J. Graciani, J. Evans, D. Stacchiola, S. D. Senanayake, L. Barrio, P. Liu, J. F. Sanz, J. Hrbek and J. A. Rodriguez, *J. Am. Chem. Soc.*, 2010, **132**, 356–363.
35 J. A. Rodriguez, S. Ma, P. Liu, J. Hrbek, J. Evans and M. Perez, *Science*, 2007, **318**, 1757–1760.
36 J. Knudsen, A. U. Nilekar, R. T. Vang, J. Schnadt, E. L. Kunkes, J. A. Dumesic, M. Mavrikakis and F. Besenbacher, *J. Am. Chem. Soc.*, 2007, **129**, 6485–6490.
37 A. A. Gokhale, J. A. Dumesic and M. Mavrikakis, *J. Am. Chem. Soc.*, 2008, **130**, 1402–1414.
38 P. Liu and J. A. Rodriguez, *J. Chem. Phys.*, 2007, **126**, 164705.
39 Q. L. Tang, Z. X. Chen and X. He, *Surf. Sci.*, 2009, **603**, 2138–2144.
40 G. J. K. Acres, J. C. Frost, G. A. Hards, R. J. Potter, T. R. Ralph, D. Thompsett, G. T. Burstein and G. J. Hutchings, *Catal. Today*, 1997, **38**, 393–400.
41 Z. J. Zhao, Z. L. Li, Y. R. Cui, H. Y. Zhu, W. F. Schneider, W. N. Delgass, F. Ribeiro and J. Greeley, *J. Catal.*, 2017, **345**, 157–169.
42 M. X. Zhou, T. N. M. Le, L. K. Huynh and B. Liu, *Catal. Today*, 2017, **280**, 210–219.
43 M. X. Zhou and B. Liu, *ChemCatChem*, 2015, **7**, 3928–3935.
44 J. A. Rodriguez, S. Ma, P. Liu, J. Hrbek, J. Evans and M. Perez, *Science*, 2007, **318**, 1757–1760.
45 X. K. Gu and W. X. Li, *J. Phys. Chem. C*, 2010, **114**, 21539–21547.
46 D. Wolf, M. Barre-Chassonnery, M. Hohenberger, A. van Veen and M. Baerns, *Catal. Today*, 1998, **40**, 147–156.
47 G. W. Huber, J. W. Shabaker, S. T. Evans and J. A. Dumesic, *Appl. Catal., B*, 2006, **62**, 226–235.
48 X. K. Gu, B. Liu and J. Greeley, *ACS Catal.*, 2015, **5**, 2623–2631.
49 T. Shishido, M. Yamamoto, D. L. Li, Y. Tian, H. Morioka, M. Honda, T. Sano and K. Takehira, *Appl. Catal., A*, 2006, **303**, 62–71.
50 P. J. Guo, L. F. Chen, Q. Y. Yang, M. H. Qiao, H. Li, H. X. Li, H. L. Xu and K. N. Fan, *Int. J. Hydrogen Energy*, 2009, **34**, 2361–2368.
51 K. Ueda, H. Tabata and T. Kawai, *Appl. Phys. Lett.*, 2001, **79**, 988–990.
52 P. Sharma, A. Gupta, K. V. Rao, F. J. Owens, R. Sharma, R. Ahuja, J. M. O. Guillen, B. Johansson and G. A. Gehring, *Nat. Mater.*, 2003, **2**, 673–677.
53 Z. W. Jin, T. Fukumura, M. Kawasaki, K. Ando, H. Saito, T. Sekiguchi, Y. Z. Yoo, M. Murakami, Y. Matsumoto, T. Hasegawa and H. Koinuma, *Appl. Phys. Lett.*, 2001, **78**, 3824–3826.
54 S. Kolesnik, B. Dabrowski and J. Mais, *J. Appl. Phys.*, 2004, **95**, 2582–2586.
55 D. A. Schwartz, N. S. Norberg, Q. P. Nguyen, J. M. Parker and D. R. Gamelin, *J. Am. Chem. Soc.*, 2003, **125**, 13205–13218.
56 G. Kresse and J. Furthmuller, *Phys. Rev. B: Condens. Matter Mater. Phys.*, 1996, **54**, 11169–11186.
57 G. Kresse and J. Furthmuller, *Comput. Mater. Sci.*, 1996, **6**, 15–50.
58 J. P. Perdew and Y. Wang, *Phys. Rev. B: Condens. Matter Mater. Phys.*, 1992, **45**, 13244–13249.
59 G. Henkelman, B. P. Uberuaga and H. Jonsson, *J. Chem. Phys.*, 2000, **113**, 9901–9904.
60 G. Henkelman and H. Jonsson, *J. Chem. Phys.*, 2000, **113**, 9978–9985.
61 S. L. Dudarev, G. A. Botton, S. Y. Savrasov, C. J. Humphreys and A. P. Sutton, *Phys. Rev. B: Condens. Matter Mater. Phys.*, 1998, **57**, 1505–1509.
62 X. K. Gu, R. Ouyang, D. Sun, H. Y. Su and W. X. Li, *ChemSusChem*, 2012, **5**, 871–878.
63 L. Giordano, G. Pacchioni, J. Goniakowski, N. Nilius, E. D. L. Rienks and H. J. Freund, *Phys. Rev. B: Condens. Matter Mater. Phys.*, 2007, **76**, 075416.
64 Q. Wang, Q. Sun, P. Jena and Y. Kawazoe, *Phys. Rev. B: Condens. Matter Mater. Phys.*, 2009, **79**, 115407.
65 P. A. Deshpande and G. Madras, *AIChE J.*, 2010, **56**, 2662–2676.
66 P. A. Deshpande, M. S. Hegde and G. Madras, *AIChE J.*, 2010, **56**, 1315–1324.
67 C. Woll, *Prog. Surf. Sci.*, 2007, **82**, 55–120.
68 B. Meyer, H. Rabaa and D. Marx, *Phys. Chem. Chem. Phys.*, 2006, **8**, 1513–1520.
69 B. Meyer, D. Marx, O. Dulub, U. Diebold, M. Kunat, D. Langenberg and C. Woll, *Angew. Chem., Int. Ed.*, 2004, **43**, 6642–6645.
70 O. Dulub, B. Meyer and U. Diebold, *Phys. Rev. Lett.*, 2005, **95**, 136101.
71 T. Bligaard, J. K. Norskov, S. Dahl, J. Matthiesen, C. H. Christensen and J. Sehested, *J. Catal.*, 2004, **224**, 206–217.

